Analysis of defrost control logic for air-source heat pumps using image and cycle data

Sumin Lee [a], Soonbum Kwon [a], Jungwoo Lee [a], Yongchan Kim [a,*]

[a]Department of Mechanical Engineering, Korea University, Seoul 02841, Republic of Korea

Abstract

Frost accumulation on the outdoor heat exchanger is a major issue for air-source heat pumps (ASHPs) operating in winter, as it blocks airflow and reduces heating capacity. Periodic defrosting is required to restore performance, but conventional time-and temperature-based defrost logic often initiates defrosting too early or too late because it does not directly measure frost accumulation. This study experimentally evaluated the limitations of conventional defrost logic using a 12 kW ASHP under various outdoor temperature and humidity conditions. A next-generation defrost initiation method was then developed by combining an image-based frosting index, the block ratio (BR), with cycle operating data. This integrated approach enables a more accurate assessment of frost formation. Results show that initiating defrosting immediately when BR reaches 1 minimizes unnecessary compressor operation. While the heating operating ratio remained nearly unchanged, the proposed logic improved heating capacity by up to 1.8% and COP by up to 3.8%. Overall, the BR-based strategy effectively reduces energy waste and enhances system efficiency.

Keywords: air-source heat pumps; block ratio; defrosting; frost formation.

1. Introduction

Air source heat pumps (ASHPs) are increasingly recognized as an energy-efficient and eco-friendly alternative to conventional heating systems, leading to significant reductions in power consumption and carbon emissions [1]. However, when operating in the heating mode during winter, condensation occurs when the outdoor evaporator surface temperature drops below 0 °C, followed by frost formation. This frost accumulation reduces the heat exchange area and heating capacity, thereby degrading the overall system efficiency. Therefore, periodic defrosting is necessary to remove the accumulated frost, which inevitably interrupts the heating operation and increases energy consumption.

Currently, most residential and commercial heat pump systems rely on simple time- and temperature-based defrost control logic. These methods do not directly evaluate the actual frost extent on the heat exchanger surface; instead, they initiate defrosting after a fixed operating time or upon reaching a specific temperature threshold. Consequently, this can result in either premature defrosting (mal-defrosting), which is initiated before sufficient frost has accumulated, or delayed defrosting, which is initiated after excessive frost accumulation. Such inaccurate defrost initiation not only wastes energy and shortens the lifespan of components but also negatively affects the user's thermal comfort due to unstable heating performance. [2] Therefore, determining the accurate defrost initiation timing is crucial to securing the high efficiency and heating performance of the heat pump.

A variety of studies have investigated the determination of defrost initiation timing. For instance, Chung et al. [3] monitored the air-side pressure difference between the heat exchanger inlet and outlet using a differential pressure sensor; defrosting is initiated when the pressure drop, caused by increased air flow resistance due to frost accumulation, exceeds a critical threshold. Tang et al. [4] proposed the time-current-temperature (T-I-T)

* Corresponding author. *E-mail address:* yongckim@korea.ac.kr

method, which detects the change in the outdoor fan's driving current caused by frost accumulation; defrosting is triggered when the current increase surpasses a threshold. Furthermore, Zhu et al. [5] utilized the temperature-humidity-time (T-H-T) method, which employs a pre-built frosting map based on ambient temperature and humidity to determine the defrosting moment. However, a common limitation of these conventional sensor-based methods is that defrosting for the entire system is initiated when the sensor value at a specific location reaches a critical threshold. Consequently, this leads to an inaccurate assessment of the frost state across the heat exchanger surface, which can result in false defrosting.

To overcome this limitation, this study proposes a next-generation defrost control logic that combines image-based frost detection technology, utilizing visual data of the outdoor coil, with cycle parameters such as refrigerant mass flow rate, pressure, and temperature. [6] The integration of visual data and cycle operating data allows for a more accurate detection of the frost state and the derivation of the optimal defrosting timing. For quantitative evaluation of the limits of conventional defrost control strategies, a 12 kW heat pump was experimentally tested under various outdoor temperature and relative humidity conditions by applying both the conventional and the proposed next-generation defrost initiation logics.

2. Experimental setup

2.1. Experimental setup and test conditions

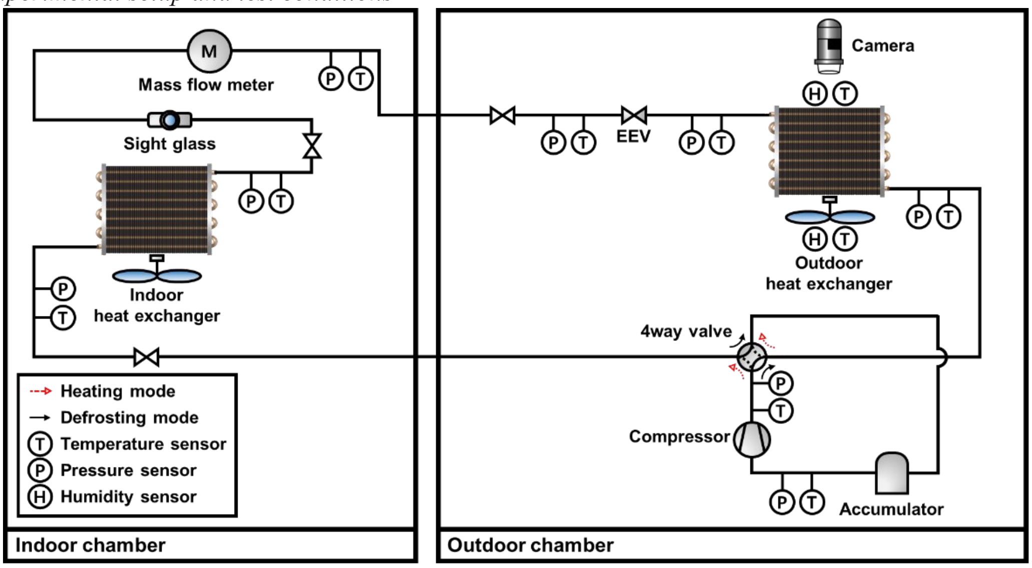

Figure 1. Schematic of experimental setup.

The experimental setup consisted of a heat pump unit situated within a psychrometric chamber. Fig. 1 shows a schematic of the experimental setup for the heat pump system. A single indoor unit and a single outdoor unit were installed in the indoor and outdoor chambers, respectively. To obtain the cycle operation data, a mass flow meter, pressure sensors, temperature sensors, and humidity sensors were installed. The sensor values were recorded and stored on a computer as excel files using a data logger. The specifications and accuracy of each measuring device are listed in Table 1. To acquire visual data, specifically the frost block ratio (BR) value, the surface of the outdoor evaporator was filmed using a video camera. The experiment was conducted under the conditions presented in Table 2. For both the conventional logic and the new logic, the following key results were derived: COP, average heating capacity, heating time, defrosting time, and heating operating ratio.

Table 1. Measurement device and accuracy.

Measured parameter	Device (model)	Range	Accuracy
Temperature	Resistance thermometer (Omega PT 100 class 1/3)	−200–600 °C	±0.10 °C
	Thermocouple (Omega T-type)	−250–350 °C	±0.40 °C
Humidity	Humidity module (E+E elektronik EE99-1)	0–100%	±1.3%
Pressure	Pressure transmitter (Allsensor P201)	0–4000 kPa	±10 kPa
Mass flow rate	Mass flow meter (Oval ALTImass CA006)	3.6–360 kg h^{-1}	±0.10%
Compressor work	Power meter (Yokogawa WT310)	0–3000 W	±0.1%

Table 2. Experimental conditions.

Parameters	Experimental case					
	Case 1	Case 2	Case 3	Case 4	Case 5	Case 6
Indoor air inlet temperature (°C)	20	20	20	20	20	20
Outdoor air inlet temperature (°C)	2	0	−2	−4	0	−2
Outdoor air inlet relative humidity (%)	90	90	90	90	80	80

2.2. Image processing

To accurately investigate the frost condition on the outdoor evaporator surface over time, videos were recorded using a camera installed on the outdoor unit. Frost images were obtained by capturing frames synchronized with the time series of the data logger. Image processing was subsequently performed to evaluate the blocking ratio (BR) of the frost from the acquired images. The overall process is illustrated in Fig. 2.

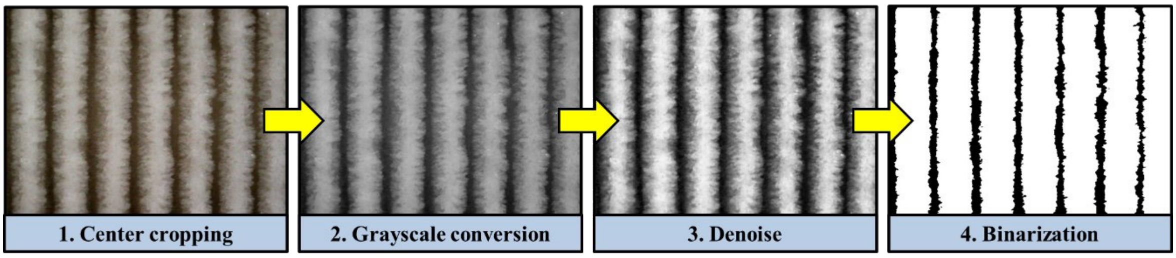

Figure 2. Image processing procedure.

The captured image consists of RGB (Red, Green, Blue) data. R, G, and B represent the brightness of each pixel and have values ranging from 0 to 255. After image processing, the image composed of only two pixel values (0 and 1), classifying each pixel as either background or object based on a threshold. If the pixel value is greater than the threshold, it is classified as the object region where frost is present, and it is assigned a value of 1; otherwise, it is considered the background where frost is absent, and it is assigned a value of 0. Therefore, the BR can be obtained by calculating the ratio of frost pixels in the binary image. The BR is the ratio of the frost area to the total image area and is calculated following the form shown in Eq. (1).

$$BR = \frac{the\ number\ of\ pixels\ in\ the\ frost\ area}{the\ total\ number\ of\ pixels\ in\ the\ image} \tag{1}$$

The BR calculated through this process is utilized to determine the defrost initiation in the next-generation control logic, which initiates defrost precisely at the point where the BR reaches 1.

2.3. Data reduction and uncertainty analysis

To quantitatively evaluate the improvement effect of the next-generation defrost initiation logic, the instantaneous heating capacity (Q_{heat}), coefficient of performance (COP), and heating operating ratio (HOR) for one cycle, including heating and defrosting, were calculated. The instantaneous heating capacity, Q_{heat}, was calculated by multiplying the mass flow rate ($\dot{m}$) obtained from the mass flow meter by the enthalpy difference across the condenser. This is shown in Eq. (3):

$$Q_{heat} = \dot{m}(h_{comp,out} - h_{cond,out}) \tag{3}$$

The enthalpies at the compressor outlet $h_{comp,out}$ and condenser outlet $h_{cond,out}$ were obtained using REFPROP, utilizing the measured pressures and temperatures. Subsequently, the average heating capacity, $Q_{heat,avg}$, is defined as the sum of instantaneous Q_{heat} values over time, divided by the total heating time (t_{heat}). The COP for one cycle is defined as the ratio of the total heating energy (Q_{heat}) delivered to the total work input for heating ($W_{comp,heat}$) and defrosting ($W_{comp,defrost}$) as shown in Eq. (4):

$$COP = \frac{Q_{heat}}{W_{comp,heat} + W_{comp,defrost}} \tag{4}$$

The heating operating ratio (HOR) is calculated as shown in Eq. (5):

$$HOR = \frac{t_{heat}}{t_{heat}+t_{defrost}} \times 100 \tag{5}$$

Here, t_{heat} represents the heating time, and $t_{defrost}$ represents the defrost time.
To evaluate the specific performance characteristics of the defrost strategies, the COP degradation rate (D_{COP}) and performance improvement rate (ξ) were introduced. The D_{COP} quantifies the efficiency loss during the saturation period (The BR reaches 1 to the start of defrosting) in the conventional logic, as shown in Eq. (6). Meanwhile, the improvement rates for the average heating capacity (ξ_Q) and COP (ξ_{COP}) represent the percentage enhancement of the new logic compared to the conventional logic, as shown in Eqs. (7) and (8):

$$D_{COP} = \frac{COP(t_{BR=1})-COP(t_{initial})}{COP(t_{BR=1})} \times 100 \tag{6}$$

$$\xi_Q = \frac{\bar{Q}_{h,new}-\bar{Q}_{h,conventional}}{\bar{Q}_{h,conventional}} \tag{7}$$

$$\xi_{COP} = \frac{\overline{COP}_{new}-\overline{COP}_{conventional}}{\overline{COP}_{conventional}} \tag{8}$$

Here, $t_{BR=1}$ and $t_{initial}$ represent the time when BR reaches 1 and defrost initiation time, respectively, $\bar{Q}_h$ and $\overline{COP}_h$ indicate the average performance values for the new and conventional logics.

Uncertainty analysis was conducted in accordance with ASHRAE Guideline 2 [7]. The total uncertainty was determined by combining systematic and random errors using the root-sum-square (RSS) method. All statistical estimates and the final uncertainty analysis were performed at a 95% confidence level. As shown in Table 3, the total errors for heating capacity and COP were found to be 0.38% and 0.45%, respectively.

Table 3. Uncertainty analysis.

Parameters	Systematic error	Random error	Total error
Compressor outlet pressure (kPa)	±0.35%	±0.04%	±0.35%
Compressor outlet temperature (°C)	±0.41%	±0.01%	±0.41%
Condenser outlet pressure (kPa)	±0.36%	±0.04%	±0.37%
Condenser outlet temperature (°C)	±0.53%	±0.03%	±0.54%
Relative humidity (%)	±1.55%	±0.17%	±1.56%
Mass flow rate (kg h^{-1})	±0.10%	±0.11%	±0.15%
Heating capacity (kW)	±0.36%	±0.11%	±0.38%
Power consumption (kW)	±0.24%	±0.04%	±0.24%
COP	±0.43%	±0.12%	±0.45%

3. Results and discussion

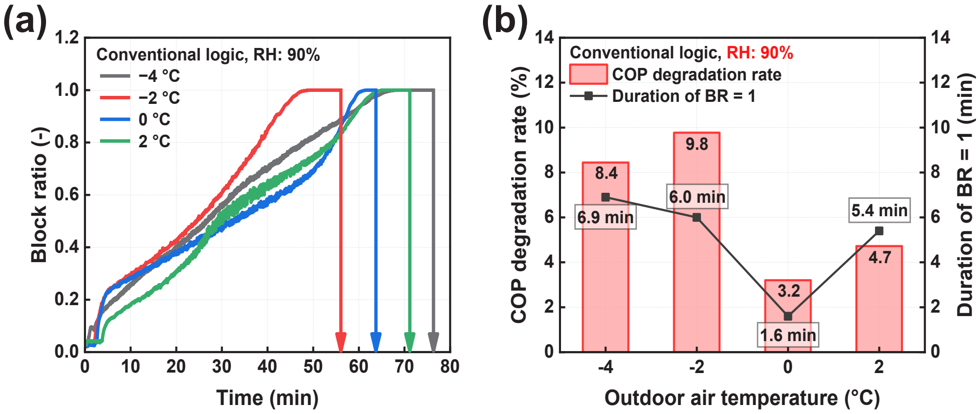

Figure 3. Conventional logic at 90% RH: (a) BR variation; (b) BR = 1 duration and COP reduction.

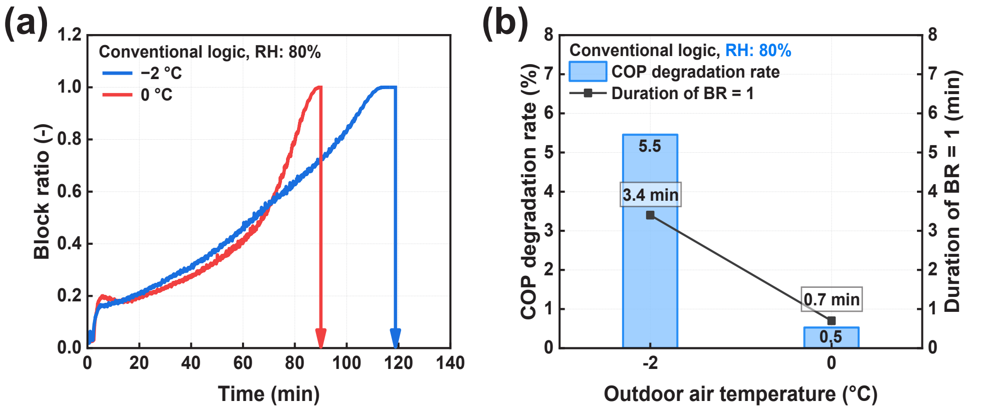

Figure 4. Conventional logic at 80% RH: (a) BR variation; (b) BR = 1 duration and COP reduction.

Fig. 3(a) shows the BR trends under the conventional defrost logic at 90% RH. In all temperature conditions, the BR increases over time and remains at BR = 1 for a noticeable duration, indicating excessive frost accumulation. This unnecessary blockage leads to performance degradation, as confirmed in Fig. 3(b). At 2 °C, the BR = 1 state lasted about 6.0 min, resulting in a 9.8% drop in COP. Although compressor frequency increases during this period, the heat exchanger capacity decreases due to full blockage, reducing overall COP.

Fig. 4(a) presents the BR behavior at 80% RH. Compared with Fig. 3(a), the BR = 1 duration is significantly shorter, demonstrating that humidity strongly influences frost growth. At 0 °C, BR = 1 lasted only 0.7 min, and the COP reduction was minimal (0.5%) because defrosting occurred before major performance degradation. These results indicate that initiating defrosting as soon as BR reaches 1 helps prevent COP loss.

Fig. 5(a) compares heating time, defrost time, and HOR between the conventional and proposed logics. Because the proposed logic triggers defrost earlier to avoid prolonged BR = 1, both heating time and defrost time decrease, resulting in a similar HOR for both logics.

Fig. 5(b) shows the improvement in average heating capacity and COP when applying the proposed logic. Since defrosting is initiated immediately at BR = 1, redundant compressor energy consumption is minimized.

As a result, COP increased by up to 3.8% at −2 °C and 90% RH, and the average heating capacity improved by up to 1.8% at −4 °C and 90% RH. Although improvements under 80% RH were smaller, slight gains were still observed. Overall, the proposed BR-based defrost logic effectively reduces unnecessary energy use and enhances system performance across varying outdoor conditions. The BR calculated through these image-processing procedures quantitatively represents the relative area covered by frost within the image and is utilized as an index for the amount of frosting.

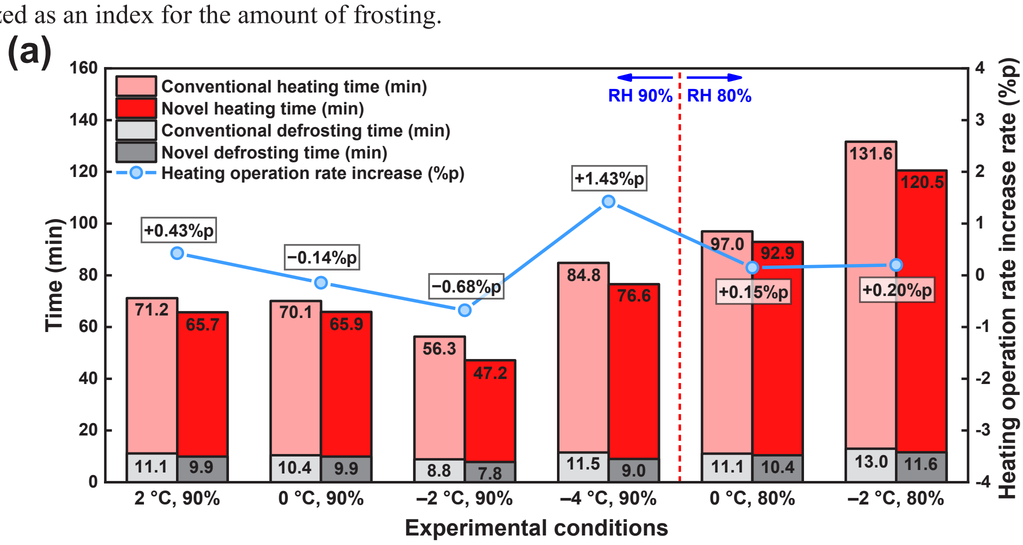

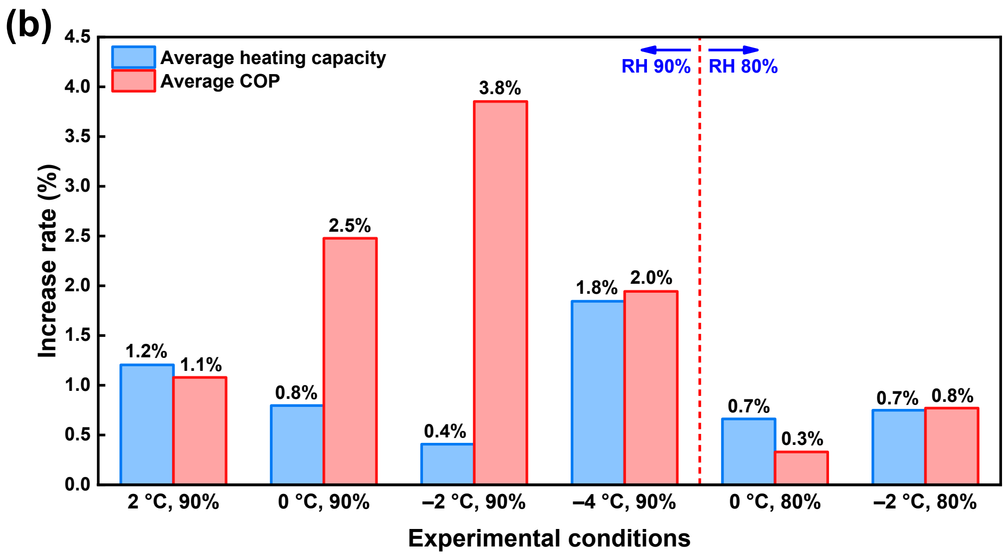

Figure 5. Comparison of conventional and proposed logics: (a) heating/defrost time and HOR; (b) average heating capacity and COP.

4. Conclusion

In this study, a next-generation defrost initiation logic combining the image-based frosting index, Block Ratio (BR), with cycle operating data was proposed. The limitations of the conventional time-temperature-based defrost logic were quantitatively verified through experiments using a 12 kW air source heat pump (ASHP). The conventional logic often resulted in the BR=1state being maintained for several minutes, causing unnecessary energy consumption and COP reduction. The proposed logic performed defrosting immediately upon the BR reaching 1, thereby minimizing the heat exchanger blockage time.

Consequently, although the heating and defrosting time decreased under all outdoor conditions, the Heating Operating Ratio was maintained. The COP showed a performance improvement of up to 3.8%, and the heating capacity improved by up to 1.8%. Overall, the next-generation defrost initiation logic effectively reduces unnecessary energy consumption and enhances system efficiency. It was also confirmed that this logic can accurately reflect the actual frosting state, unlike existing sensor-based methods.

Future work will focus on developing a correlation to predict BR in real-time without a camera. This equation will incorporate dominant frost variables and geometric factors—specifically fin pitch, fin height, and fan frontal area—to ensure it can be applied to various heat pump systems.

References

[1] Vorushylo I, Keatley P, Shah N, Green R, Hewitt NJ. How heat pumps and thermal energy storage can be used to manage wind power: A study of Ireland. Energy 2018;157:539–549.
[2] Klingebiel J, Höges C, Göbel S, Bannmüller P, Boelsen T, Venzik V, Vering C, Müller D. Optimal defrost initiation for air-source heat pumps: Evaluating the improvement potential of common defrosting controllers. Energy 2025;324:135037.
[3] Chung Y, Na SI, Choi J, Kim MS. Feasibility and optimization of defrosting control method with differential pressure sensor for air source heat pump systems. Applied Thermal Engineering 2019;155:461–469.International Topical Meeting on High Temperature Reactor Technology. Beijing, China, paper #B08.
[4] Tang R, Zhao Y, Deng S, et al. A novel time-current-temperature difference (T-I-T) defrosting control method for air source heat pump based on outdoor fan operation characteristics. Applied Thermal Engineering 2025;262:125189.
[5] Zhu J, Sun Y, Wang W, Ge Y, Li L, Liu J. A novel temperature–humidity–time defrosting control method based on a frosting map for air-source heat pumps. International Journal of Refrigeration 2015;54:45–54.
[6] Zhao H, Li P, Li J, Liu Z, Sang Y, Ye T, Zheng W. Applying neural network model to real-time frosting detection and intelligent defrosting control for air source heat pump. Applied Energy 2025;377:124418.
[7] ASHRAE. ASHRAE Guideline 2: Engineering Analysis of Experimental Data. Atlanta (GA, USA); 2010.